

Dominance of 2-Minute Oscillations near the Alfvén Surface

ZESAN HUANG (黄泽森) ¹, MARCO VELLI ¹, CHEN SHI (时辰) ¹, YINGJIE ZHU (朱英杰) ², B. D. G. CHANDRAN ³,
TREVOR BOWEN ⁴, VICTOR RÉVILLE ⁵, JIA HUANG (黄佳) ⁴, CHUANPENG HOU (侯传鹏) ⁶, NIKOS SIOULAS ⁴,
MINGZHE LIU (刘明哲) ⁴, MARC PULUPA ⁴, SHENG HUANG (黄胜) ⁷ AND STUART D. BALE ^{8,4}

¹Department of Earth, Planetary, and Space Sciences, University of California, Los Angeles, CA, USA

²Physikalisch Meteorologische Observatorium, Davos, World Radiation Center (PMOD/WRC), 7260 Davos, Switzerland

³Space Science Center and Department of Physics, University of New Hampshire, Durham, NH 03824, USA

⁴Space Sciences Laboratory, University of California, Berkeley, CA 94720-7450, USA

⁵IRAP, Université Toulouse III—Paul Sabatier, CNRS, CNES, Toulouse, France

⁶Institut für Physik und Astronomie, Universität Potsdam, Potsdam, Germany

⁷Center for Space Physics, Boston University, Boston, MA, USA

⁸Physics Department, University of California, Berkeley, CA 94720-7300, USA

ABSTRACT

Alfvén waves, considered one of the primary candidates for heating and accelerating the fast solar wind, are ubiquitous in spacecraft observations, yet their origin remains elusive. In this study, we analyze data from the first 19 encounters of the Parker Solar Probe (PSP) and report dominance of 2-minute oscillations near the Alfvén surface. The frequency-rectified trace magnetic power spectral density (PSD) of these oscillations indicates that the fluctuation energy is concentrated around 2 minutes for the “youngest” solar wind. Further analysis using wavelet spectrograms reveals that these oscillations primarily consist of outward-propagating, spherically polarized Alfvén wave bursts. Through Doppler analysis, we show that the wave frequency observed in the spacecraft frame can be mapped directly to the launch frequency at the base of the corona, where previous studies have identified a distinct peak around 2 minutes (~ 8 mHz) in the spectrum of swaying motions of coronal structures observed by SDO AIA. These findings strongly suggest that the Alfvén waves originate from the solar atmosphere. Furthermore, statistical analysis of the PSD deformation beyond the Alfvén surface supports the idea of dynamic formation of the otherwise absent $1/f$ range in the solar wind turbulence spectrum.

Keywords: Solar Wind, Coronal Heating, Turbulence, Alfvén Waves

1. INTRODUCTION

The heliosphere is formed by the supersonic plasma flow known as the solar wind, originating from the Sun. Parker (Parker 1958) successfully predicted the existence of this supersonic flow, which was later confirmed by *in situ* observations from the Luna 2 (Gringauz et al. 1962) and Mariner II spacecraft (Neugebauer & Snyder 1966). However, it was soon recognized (Parker 1965) that thermal conduction alone cannot accelerate the solar wind to the observed high speeds ($\gtrsim 700$ km/s), implying the need for an additional source of momentum and energy that persists into the supersonic regions of the wind (Leer & Holzer 1980).

Large-amplitude spherically polarized Alfvénic fluctuations are ubiquitous in the solar wind (Unti & Neugebauer 1968; Belcher & Davis 1971; Bale et al. 2019;

Kasper et al. 2019; Drake et al. 2021; Larosa et al. 2021; Shi et al. 2022b; Telloni et al. 2022; Jagarlamudi et al. 2023; Huang et al. 2023a). As the name says they are characterized by a quasi-constant magnetic magnitude $|B|$, and the tip of the magnetic field vector undergoes a random walk on a sphere (Barnes & Hollweg 1974; Tsurutani et al. 1997; Matteini et al. 2014, 2024). In addition the very high velocity-magnetic field correlation corresponds to that of waves propagating away from the sun. The constant $|B|$ state is an exact solution of the magnetohydrodynamics (MHD) equations, which can propagate without much nonlinear interaction. Thus, the Alfvén wave is considered to be a prime candidate for the heating and acceleration of the solar wind (Belcher 1971; Belcher & Olbert 1975; Alazraki &

Couturier 1971; Hansteen & Velli 2012; Shi et al. 2022a; Rivera et al. 2024).

However, the origin of solar wind Alfvénic fluctuations remains a subject of debate (Banerjee et al. 2021). Some suggest they are generated by magnetic reconnection in the lower solar corona (Bale et al. 2021; Drake et al. 2021; Bale et al. 2023), while others argue that Alfvén waves originate deeper in the solar atmosphere (Jess et al. 2009, 2015; Morton et al. 2023). These deeper sources may include the transition region and chromosphere (Tian et al. 2014; De Pontieu et al. 2007; Kuridze & Zaqarashvili 2008; Hou et al. 2024), or even the photosphere, where they could be generated by p-mode oscillations (Ulrich 1970) and reach the corona through double mode conversion (Cally 2012; Hansen & Cally 2012; Morton et al. 2013, 2015; Cally 2017; Morton et al. 2019; Kuniyoshi et al. 2023), or through buffeting of magnetic flux tubes in “G band bright points” by convective motions (Cranmer & Ballegooijen 2005; Ballegooijen & Asgari-Targhi 2016). Therefore, leveraging state-of-the-art *in situ* observations is crucial for constraining existing theories.

Parker Solar Probe (PSP) was launched in late 2018 (Fox et al. 2016). Since then, it has been providing *in situ* observations from the magnetically dominated solar corona (Kasper et al. 2021; Chhiber et al. 2024). The unprecedented data from distances to the Sun smaller than 0.25 AU has ushered in a new era of solar wind turbulence studies (see, e.g., Chen et al. (2020); Shi et al. (2021); Zhao et al. (2021); Matthaeus (2021); Sioulas et al. (2022); Zank et al. (2022); Zhang et al. (2022a); Sioulas et al. (2023a,b); Dunn et al. (2023); Larosa et al. (2023); McIntyre et al. (2023), and Raouafi et al. (2023) for a recent review). In the standard solar wind turbulence model for the fast wind (Bruno & Carbone 2013), the trace magnetic power spectral density is characterized by a “ $1/f$ -inertial” double power law, where the $1/f$ range at low frequencies is known as the energy-containing range. However, one of the surprising discoveries of PSP is the systematic absence of the low-frequency $1/f$ range near the Alfvén surface (Huang et al. 2023b; Davis et al. 2023), i.e. the region where the solar wind flow overtakes the Alfvén speed as it accelerates outwards (Kasper et al. 2021; Chhiber et al. 2024). Instead, the turbulence spectrum is predominantly characterized by a “shallow-inertial” double power law, where the shallow part scales like $f^{-0.5}$. Beyond, in the super-Alfvénic wind, the $1/f$ range gradually forms between the shallow and inertial part of the spectrum, creating a “shallow- $1/f$ -inertial” triple power law. As the solar wind travels outwards, the spectrum will eventually transform into the tradi-

tional “ $1/f$ -inertial” scaling. As will be elaborated in this paper, the “shallow-inertial” scaling and its deformation have significant implications on the distribution of fluctuation energy in the spectrum.

In this paper, we report the dominance of 2-minute oscillations in the trace magnetic power spectral density near the Alfvén surface. The paper is organized as follows: In §2, we introduce the data from PSP and examine the implications of the dominant “shallow-inertial” double power law near the Alfvén surface. We also define a statistical factor, f_{mid} , to capture the radial deformation of the spectrum. In §3, we establish a connection between the temporal signals measured in the spacecraft frame and the waves launched from the base of the corona. In §4, we show the radial evolution of $1/f_{mid}$ in the solar wind. In §5, we discuss the implications of our results and conclude our study.

2. DATA AND METHODOLOGY

2.1. Data

We use magnetic field data from the fluxgate magnetometer in the FIELDS instrument suite (Bale et al. 2016; Bowen et al. 2020) and plasma moments from SPAN-ion in the SWEAP instrument suite (Kasper et al. 2016). In this study, we treat the radial component of the first-order proton moment as the solar wind speed. On PSP, electron number density data from Quasi-Thermal-Noise (QTN) spectroscopy serve as a critical calibration standard for scientific analysis (e.g., Kasper et al. 2021; Zhao et al. 2021; Liu et al. 2021a,b, 2023; Zheng et al. 2024), especially given that the alpha-particle abundance is often negligible (2% - 6%) (Mostafavi et al. 2022). Therefore, we use electron number density data derived from the QTN technique (e.g., Moncuquet et al. 2020; Kruparova et al. 2023) as a proxy for proton number density in the solar wind.

2.2. Example Interval and Methodology

Figure 1 shows an example interval from PSP’s E17 perihelion. The interval of interest is highlighted with the pink shade from panels (c) to (h). In panel (c), we show the RTN components and magnitude of the magnetic field vector. In panel (d), we show the time-periodic trace magnetic spectrogram compiled using wavelet transformation. To convey visually the contributions to the total fluctuation energy from different range of $\ln(f)$, the power spectral density $P(f)$ is rectified with f because $P(f) df = fP(f) d \ln f$ (see also Liu et al. 2007). The black dashed curve marking the boundary of the shaded area is the Cone of Influence (CoI), which indicates the region where the wavelet falls out of the boundary for a given frequency. In panel (e), we

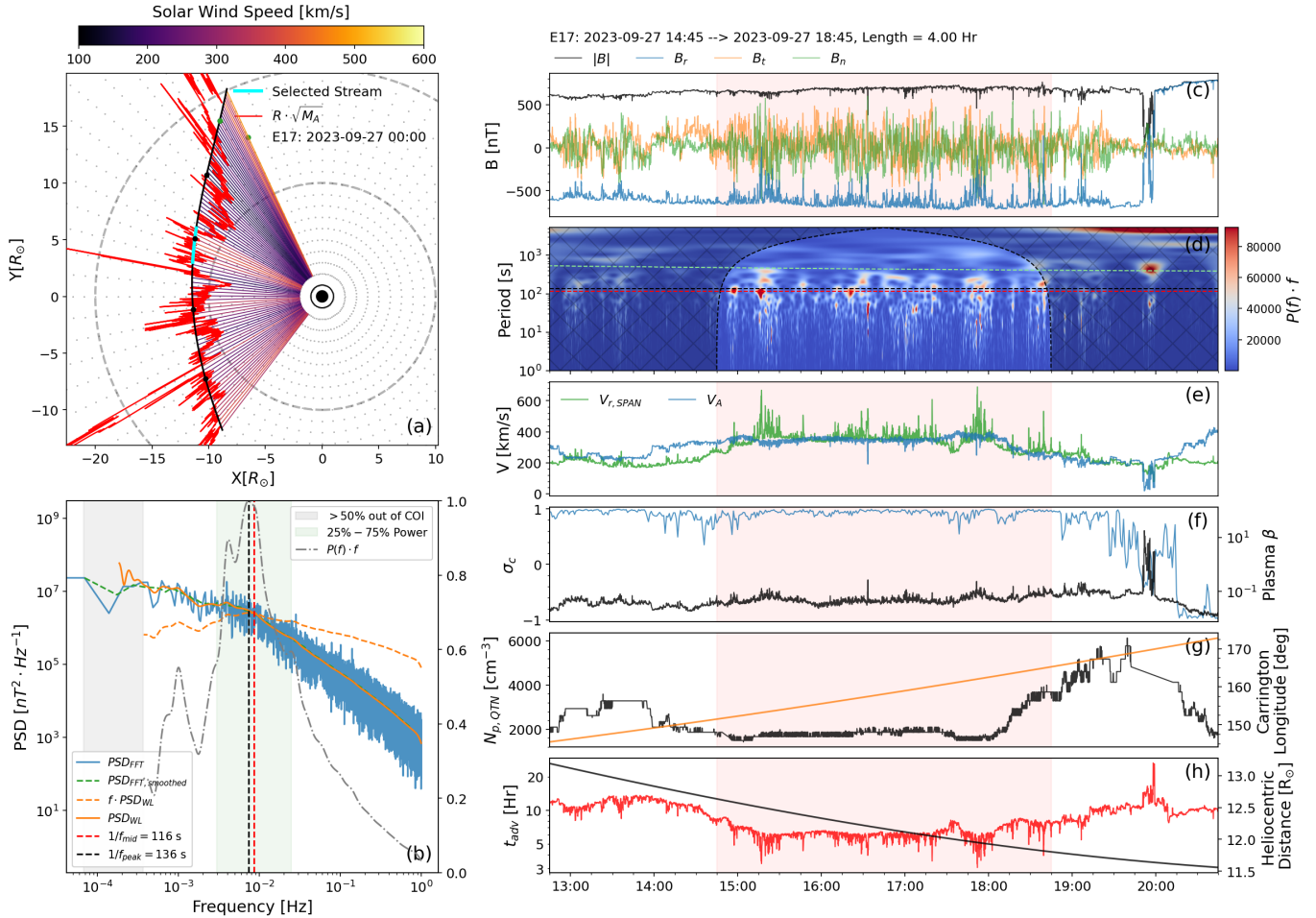


Figure 1. (a) Trajectory of PSP in the solar corotating frame. (b) Trace magnetic power spectrum density (PSD) of the selected interval. (c) R, T, N components and magnitude of the magnetic field. The selected interval is highlighted with the vertical pink area. (d) Trace wavelet scalogram of the magnetic field from the selected interval. (e) Radial solar wind V_r and Alfvén speed V_A . (f) Cross helicity σ_c (left, blue) and plasma $\beta = 2\mu_0 P/B^2$ (right, black). (g) Proton density n_p (left, black) and Carrington Longitude (right, orange) (h) Advection time $\tau_{adv} = (R - R_\odot)/V_r$ (left, red) and Heliocentric Distance R of the spacecraft (right, black).

show both the radial component of the bulk proton velocity V_r and the local Alfvén speed $V_A = |B|/\sqrt{\mu_0 m_p n_p}$ (where n_p is assumed to be the same as n_e estimated from QTN). For this specific interval, $V_r/V_A \simeq 1$, indicating that PSP is situated in the neighborhood of the Alfvén surface (Kasper et al. 2021; Chhiber et al. 2024). From panel (f) to (h), we show various plasma parameters, including cross helicity σ_c ($\sigma_c = \frac{z^{+2} - z^{-2}}{z^{+2} + z^{-2}}$, where $z^\pm = \delta\vec{V} \mp \delta\vec{B}/\sqrt{\mu_0 m_p n_p}$ are the Elsässer variables), plasma β ($\beta = 2\mu_0 P/B^2$), proton number density n_p , Carrington longitude, PSP’s heliocentric distance R , and advection time $t_{adv} = (R - R_\odot)/V_r$.

Within the interval, the amplitudes of the magnetic vector fluctuations are very large, but the magnetic field magnitude remains relatively constant. Meanwhile, σ_c remains very close to unity. The near-perfect

anti-correlation between B_r (blue curve, panel (c)) and V_r (green curve, panel (e)) indicates that the fluctuations are unidirectional, outward-propagating, large-amplitude spherically polarized Alfvén waves. Recently, these waves have been reported as the major energy source for heating and acceleration of the solar wind (Rivera et al. 2024).

The trajectory of PSP is plotted in the Carrington corotating frame (with the 27-day Carrington rotation subtracted) in panel (a), where the interval of interest is highlighted with the cyan bar (“selected stream”). The local radial solar wind speed (V_r in panel (e)) is shown by the color of the radial lines. To indicate the location of the Alfvén surface, the Alfvén Mach number ($M_A = V_r/V_A$) is visualized as the red curve. Whenever the red curve dips below the black curve, PSP is inside the magnetically dominant solar corona. To aid the

readers, the starts of each day are shown as black dots, the black dashed circles are plotted every $10 R_{\odot}$, and the radial dotted lines are plotted at 5-degree intervals in Carrington longitude.

Following previous work (Huang et al. 2023b), in this study we primarily focus on the trace power spectral density (PSD) of the magnetic field vector, shown in panel (b). The PSD_{FFT} (blue curve) is estimated using Fast Fourier Transformation (FFT). Due to the mathematical properties of FFT, PSD_{FFT} is naturally noisy. Following the procedure used in previous works (Sioulas et al. 2023a,b; Huang et al. 2023b), we smooth PSD_{FFT} with a sliding window with a frequency factor of 2, and the smoothed spectrum is $PSD_{FFT,smoothed}$ (green dashed line). However, the trajectory in panel (a) shows that PSP travels very quickly during perihelion. For the interval of interest (cyan bar), PSP traversed about 14 degrees over 4 hours. Thus, the time series measured by PSP around perihelion is highly non-stationary, violating one of the fundamental assumptions of Fourier transformation. The non-stationary effects primarily influence the low-frequency part of the spectrum. To assess the extent of these effects, we plot the averaged wavelet PSD (PSD_{WL}), shown as the orange line (averaged over the data within the CoI in panel (d)). Clearly, PSD_{WL} and $PSD_{FFT,smoothed}$ overlap perfectly in the high-frequency range and begin to diverge around $10^{-3.5}$ Hz, where a significant portion of the data fall outside the CoI. Consequently, we rely on the spectrum down to the frequency where more than 50% of the data fall outside the CoI ($f_{CoI,50\%}$), indicated by the gray shade in panel (b). For the remainder of this work, we will use PSD_{WL} as the "primary" PSD of the magnetic field time series (henceforth referred to as PSD_{WL} or $P(f)$ interchangeably), and we will extract factors from PSD_{WL} .

PSD_{WL} , as mentioned previously, is characterized by a "shallow-inertial" double power-law scaling. In the low-frequency range, the spectrum is shallower than $1/f$, and in the high-frequency range, the scaling is consistent with established turbulence phenomenology theories (e.g., Kraichnan 1965; Iroshnikov 1964; Goldreich & Sridhar 1995, 1997; Boldyrev 2005, 2006; Chandran et al. 2015), and hence it is identified as the turbulence inertial range. One interval with a spectrum shallower than $1/f$ was seen in Helios observations of fast solar wind at 0.3 AU (Tu & Marsch 1995; Chandran 2018). Recently, based on the new observations from PSP at much closer distances to the Sun ($R < 0.3AU$), this type of spectrum unexpectedly dominates, and it gradually develops into the typical " $1/f$ -inertial" spectrum as R increases (Huang et al. 2023b; Davis et al. 2023).

The "shallow-inertial" double power-law has an interesting property. It is well known that $1/f$ scaling indicates that energy is distributed evenly across different frequencies on a logarithmic scale (Keshner 1982). In other words,

$$\int_{f_1}^{f_2} \frac{1}{f} df = \ln(f_2/f_1) \quad (1)$$

is dependent only on the ratio of the integration bounds, i.e., f_2/f_1 . Given that the spectrum scales as $P(f) = f^{-\alpha}$, if $\alpha > 1$, the fluctuation energy concentrates at the low-frequency end; and when $\alpha < 1$, the energy concentrates at high frequencies. Consequently, the "shallow-inertial" scaling indicates that the energy concentrates around the "bend". To substantiate our argument, we consider a fixed window in $\ln(f)$. The energy stored in the moving window is:

$$\int P(f) df = \int P(f)f d \ln(f) \quad (2)$$

Thus, the rectified spectrum $P(f) \cdot f$ curve is proportional to the "energy density" of frequency f on a logarithmic scale. Additionally, the area under the $P(f) \cdot f$ curve in a linear-log plot represents the relative amount of fluctuation energy for a given frequency range.

In panel (b), $P(f) \cdot f$ is plotted in both logarithmic scale (orange dashed curve) and linear scale (black dotted-dashed curve, right-hand side twin axis). The logarithmic plot clearly shows that the turbulence scaling is shallower than $1/f$ in the low-frequency range ($f < 10^{-2}$ Hz, orange curve goes up) and steeper than $1/f$ in the high-frequency inertial range ($f > 10^{-2}$ Hz, orange curve goes down). Thus, $P(f) \cdot f$ peaks at $1/f_{peak} = 136$ s, indicated by the vertical black dashed line. The area under the black dotted-dashed $P(f) \cdot f$ curve represents the relative amount of total fluctuation energy. A green shade is overlaid to indicate the frequency range containing the middle 50% of the total fluctuation energy, estimated from the highest frequency f_0 down to the right-hand edge of the gray shade $f_{CoI,50\%}$. In other words, the area under the $P(f) \cdot f$ curve in the green shade contains 50% of the total area, with the right side up to f_0 containing 25%, and the left side down to $f_{CoI,50\%}$ containing the remaining 25%. The middle frequency of the green shade is named f_{mid} and is calculated to be $1/f_{mid} = 116$ s. Both f_{mid} and f_{peak} are indicated by red and black dashed lines in panels (b) and (d).

In this case, the values of f_{peak} and f_{mid} are very close, and the majority of the fluctuation energy concentrates around them (50% within the green shade). Thus, both can be considered as a "representative fre-

quency” of this interval. However, f_{peak} is very sensitive to the specific choice of interval. For example, when the spectrum gradually deforms from “shallow-inertial” to “ $1/f$ -inertial”, f_{peak} will rapidly migrate to $f_{CoI,50\%}$ (the lowest trustable frequency, as $P(f) \cdot f$ monotonically decreases as a function of f). On the other hand, f_{mid} will slowly migrate to the left as the spectrum deforms, because it represents the center of the frequency range containing the middle 50% of the total fluctuation energy (see Davis et al. (2023) for details of the deformation in E10, and Huang et al. (2023b) for a statistical analysis). Thus, f_{mid} can capture the overall deformation of the spectrum. In this study, we will use f_{mid} as the primary factor for statistical analysis.

3. INTERPRETATION OF TIME SERIES

The frequencies considered in the previous section are measured in the spacecraft frame. Thus, proper interpretation of the spacecraft time series is pivotal to our study. Generally speaking, there are two approaches to interpret the spacecraft time series: (1) directly interpret time series as temporal signals in the spacecraft frame; or (2) invoke the Taylor Hypothesis (Taylor 1938; Perez et al. 2021) and translate temporal signals into spatial signals. To make meaningful comparisons with anisotropic turbulence phenomenologies (e.g., Kraichnan 1965; Iroshnikov 1964; Goldreich & Sridhar 1995, 1997; Boldyrev 2005, 2006; Chandran et al. 2015), one must transform the frequency spectrum into the wavevector spectrum. Therefore, the latter approach is more commonly used in the solar wind turbulence community (e.g., Horbury et al. 2012; Oughton et al. 2015; Duan et al. 2021; Adhikari et al. 2021; Zhang et al. 2022b; Bandyopadhyay et al. 2022; Andrés et al. 2022; Zank et al. 2022; Sioulas et al. 2023a).

In this study, we take the first approach. We aim to establish a connection between the waves launched from the base of the corona and the waves measured by PSP near the Alfvén surface. In this section, we will show that the Alfvén wave frequency observed in the spacecraft frame can be considered identical to the launch frequency for the scenarios considered in this study.

3.1. One Dimensional Solar Wind Model

To begin, we consider a simple 1D solar wind model in the solar corotating frame, similar to earlier studies (Heinemann & Olbert 1980; Hollweg et al. 1982; Velli 1993). In this model, we ignore the perpendicular movement of PSP and consider only its radial speed, $V_{PSP,r}$.

There are three reference frames involved: the Solar surface frame, K_{\odot} , the solar wind (intrinsic) plasma frame, K_{wind} , which moves at speed U relative to K_{\odot} ,

and the PSP frame, K_{PSP} , which moves at speed $V_{PSP,r}$ relative to K_{\odot} . Similar to previous 1D models, we launch Alfvén waves at the base of the corona with a frequency f_0 . The frequency of the waves in K_{wind} is:

$$f_{wind} = f_0 \frac{V_A}{U + V_A} \quad (3)$$

where V_A is the local Alfvén speed. Similarly, the frequency of the waves in K_{PSP} is:

$$\begin{aligned} f_{PSP} &= f_{wind} \frac{U + V_A - V_{PSP,r}}{V_A} \\ &= f_0 \frac{U + V_A - V_{PSP,r}}{U + V_A} \end{aligned} \quad (4)$$

Obviously, f_{PSP} reduces to f_0 when $V_{PSP,r} \ll U + V_A$. Due to the spatial gradient of both U and V_A from the base of the corona to PSP, a substantial portion of the Alfvén waves could be reflected. In this study, we are particularly interested in the behavior of the Alfvén waves observed near the Alfvén surface (e.g., Figure 1). Thus, following Velli (1993), we will solve for the transmission coefficient profile for outward-propagating Alfvén waves from the base of the corona to the Alfvén surface.

Here we use a classical Alfvén speed and solar wind speed profile (Velli et al. 1991):

$$\rho = \rho_0 \frac{\exp\{-\alpha/2 \cdot [1 - (R_{\odot}/R)]\}}{\{1 + \beta[(R/R_{\odot} - 1)]\}^2} \quad (5)$$

$$V_A = V_{A0} \left(\frac{R_{\odot}}{R}\right)^2 \left(\frac{\rho_0}{\rho}\right)^{1/2} \quad (6)$$

$$U = \frac{U_{\infty}}{\beta^2} \exp(-\alpha/2) \left(\frac{R}{R_{\odot}}\right)^2 \left(\frac{V_A}{V_{A0}}\right)^2 \quad (7)$$

where V_{A0} is the initial Alfvén speed at the base of the corona, U_{∞} is the asymptotic solar wind speed at infinity, and α and β are free parameters. As an example, we choose the following parameters: $\alpha = 0, \beta = 5.6, V_{A0} = 1000$ km/s, $U_{\infty} = 500$ km/s. Our choice produces an Alfvén surface at $12R_{\odot}$ with $U = V_A = 434$ km/s, consistent with PSP observations in Figure 1. The profiles of U , V_A , and $U + V_A$ are shown in Figure 2.

To obtain the transmission coefficient profile, we solve the linear propagation equation for the two Elsässer variables:

$$\begin{aligned} -i\omega z^{\pm} + (\vec{U} \pm \vec{V}_A) \cdot \nabla z^{\pm} + z^{\mp} \cdot \nabla(\vec{U} \mp \vec{V}_A) \\ + \frac{1}{2}(z^{-} - z^{+})\nabla \cdot (\vec{V}_A \mp \frac{1}{2}\vec{U}) = 0 \end{aligned} \quad (8)$$

where ω is the angular frequency of the wave in the solar wind frame at distance R . The transmission coefficient is defined in terms of the total wave action flux, which

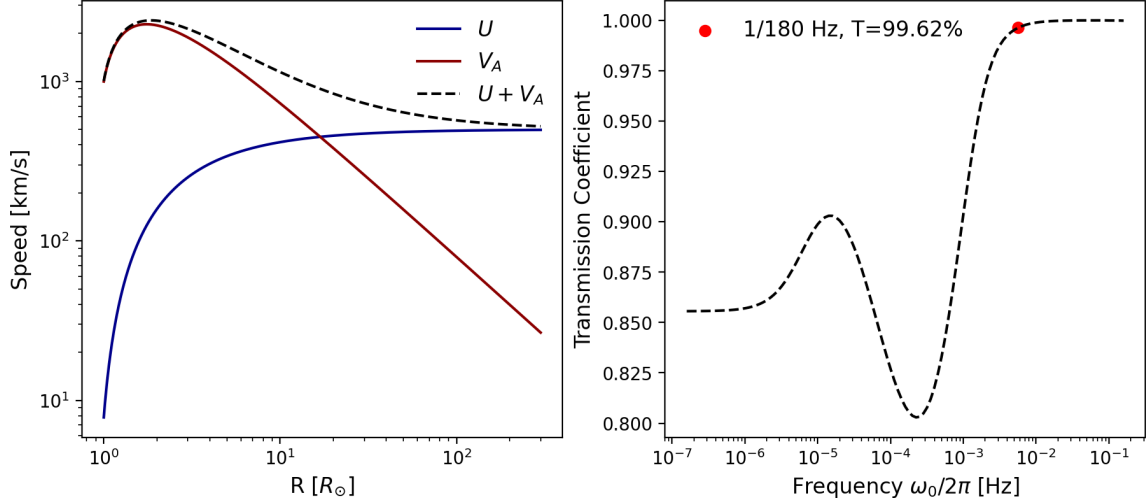


Figure 2. Left: Solar wind and Alfvén speed profile. Right: Transmission coefficient of Alfvén waves as a function of launch frequency.

is otherwise conserved in the WKB (Wentzel-Kramers-Brillouin) limit:

$$S^\pm = \frac{1}{2} \rho \frac{(z^\pm/2)^2}{\omega_0 \frac{V_A}{U \pm V_A}} \cdot (U \pm V_A) \cdot A \quad (9)$$

where A is the cross-sectional area of the flux tube. Note that here the wave action density (see e.g., Bretherton 1968; Dewar 1970) is defined as the energy density divided by the wave frequency ω in the solar wind frame:

$$\frac{1}{2} \rho \frac{(z^\pm/2)^2}{\omega} = \frac{1}{2} \rho \frac{(z^\pm/2)^2}{\omega_0 \frac{V_A}{U \pm V_A}}$$

where ω is Doppler-shifted downward compared to the launch frequency ω_0 due to the presence of the wind. There are two important properties of (8): First, the net outward-propagating wave action flux is conserved:

$$S^+ - S^- = S_\infty = S_c \quad (10)$$

where S_∞ is the total wave action flux at infinity, and S_c is the flux at the Alfvén surface ($S^- = 0$ at the Alfvén surface because $U = V_A$). The transmission coefficient for a given launch angular frequency ω_0 is then defined as:

$$T = \frac{S_c}{S_0^+} \quad (11)$$

where S_0^+ is the total wave action flux at the base of the corona. Second, the singular point at the Alfvén surface ($U = V_A$) provides a natural boundary condition for the system. At this singular point, (8) reduces to:

$$-i\omega z^- + \frac{1}{2}(z^- - z^+) \nabla \cdot (\vec{V}_A + \frac{1}{2} \vec{U}) = 0 \quad (12)$$

Now, combining (8) - (12), we integrate the transmission coefficient from the given U and V_A profiles, and the result is shown in the right panel of Figure 2.

We may now examine the Doppler shift effects from the radial movements of PSP and the transmission coefficient of the “representative frequency” found in Figure 1. Around the Alfvén surface, $V_{PSP,r} \lesssim 100$ km/s, and $U + V_A \gtrsim 800$ km/s (Figure 1(e)). Thus, the radial Doppler shift factor:

$$\frac{U + V_A - V_{PSP,r}}{U + V_A} \sim 1$$

is mostly negligible, and the effect is strongest during the fast radial scan phase. The “representative frequency” in Figure 1 lies between 2 to 3 minutes. This indicates that the launch frequency of these Alfvén waves at the solar surface should be similar. From the right panel of Figure 2, we can see that the transmission coefficient for a 3-minute Alfvén wave from the base of the corona to the Alfvén surface is very close to unity. Thus, based on our 1D solar wind model, the 2-3 minute Alfvén waves could be launched from the base of the corona and reach PSP around the Alfvén surface without significant reflection.

However, the analysis above has ignored two very important effects: the perpendicular movement of PSP and nonlinear interactions. In the following subsection, we address the first effect, and in the discussion section, we will examine the second effect.

3.2. Perpendicular Contamination

The perpendicular motion of the Parker Solar Probe (PSP) causes a Doppler shift that transforms spatial structures into temporal signals, potentially contaminating time series in the spacecraft’s frame of reference.

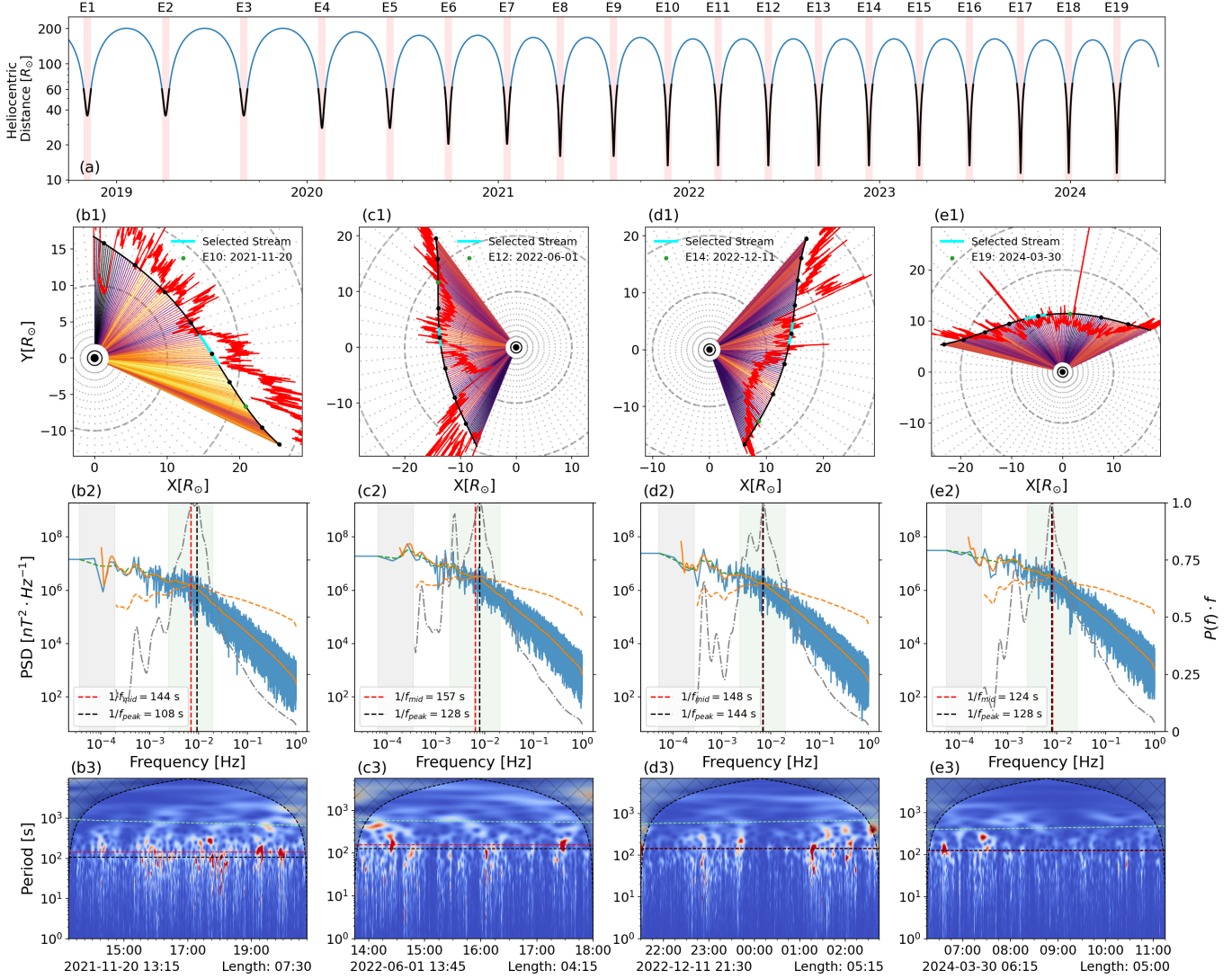


Figure 3. (a) Heliocentric distance of PSP as of Jul-01-2024. The time range considered in this study are highlighted with the black lines and pink shaded area. (b1-e1) Trajectory of PSP (black line) in Carrington corotating frame. (b2-e2) Power spectrum density of the selected interval. (b3-e3) Wavelet scalogram of trace magnetic field power spectrum of the selected interval. The elements in (b), (c) and (d) are identical to Figure 1 (a), (b) and (d).

This Doppler shift is described by the following relation:

$$2\pi f = k_{\phi} \cdot V_{PSP,\phi} \quad (13)$$

where k_{ϕ} is the wavenumber of the spatial structures in the perpendicular ϕ direction. The power spectral density of the perpendicular wavenumber $P(k_{\phi})$ is an unknown function. However, it is well established that Alfvén waves are guided by the background magnetic field, and around the Alfvén surface, this field is predominantly radial. Therefore, the perpendicular spatial signals are likely caused by crossings of intermittent flux tubes. Despite this, it is highly improbable that the concentration of 2-minute oscillations results from perpendicular contamination for two primary reasons.

First, Figure 1(d) shows that the oscillations are highly localized in the wavelet spectrogram. In other words, the dominant contributors to the peak in the rectified $P(f) \cdot f$ spectrum are the few wave bursts (“red islands” in panel (d)). This feature of the waves further supports the temporal nature of the signals, rather than contamination from the Doppler shift of spatial structures. To reinforce the universality of this observation, we present four additional example intervals in Figure 3. All of these intervals are located near the Alfvén surface, and the oscillations remain highly localized in the time-period domain.

Second, for a fixed size at the coronal base, the Doppler-shifted frequency depends on the local ratio $V_{PSP,\phi}/R$. This ratio varies significantly through-

out each perihelion since $V_{PSP,\phi}$ increases as PSP approaches perihelion. To illustrate this effect, we calculate an example of the perpendicular contamination frequency based on the size of a solar granule $\lambda_{granule} = 1700$ km (Rieutord et al. 2010), assuming a super-radial expansion factor of 3:

$$f_c = \frac{V_{PSP,\phi}}{3\lambda_{granule} \cdot R/R_\odot} \quad (14)$$

This frequency is represented by green dashed lines in the wavelet spectrograms of Figures 1 and 3. In Figure 3(b), PSP is nearing the end of its fast radial scan phase, where $R \simeq 17R_\odot$. Here, $V_{PSP,\phi} \simeq 100$ km/s, yielding $1/f_c \sim 1000$ s. In Figure 3(e), as PSP moves closer to perihelion, $R \simeq 12R_\odot$ and $V_{PSP,\phi} \simeq 150$ km/s, leading to $1/f_c \sim 400$ s. Despite these changes, the peaks of the fluctuation energy across all five intervals remain consistent, close to 2 minutes. This suggests that to consistently produce the 2-minute peaks, flux tubes at the coronal base must fine-tune their sizes according to the local ratio of $V_{PSP,\phi}/R$. Additionally, even for locally generated structures, they must adjust their sizes to account for variations in $V_{PSP,\phi}$, which can fluctuate by at least 50% across the intervals with 2-minute peaks. Achieving such consistent 2-minute peaks under these conditions would be quite remarkable.

In summary, in this section, we have established a connection between the Alfvén waves launched from the base of the corona and the Alfvén waves measured by PSP near the Alfvén surface. The bursty nature of the Alfvén waves provides strong evidence that they are temporal signals rather than Doppler-shifted spatial structures. In the following section, we will conduct a statistical analysis of f_{mid} to understand its radial evolution in the solar wind.

4. STATISTICAL RESULTS

To investigate the evolution of f_{mid} in the solar wind, we perform a statistical analysis of data from the first 19 encounters of the Parker Solar Probe (PSP). We consider data from ± 7 days around each perihelion, as highlighted in Figure 3(a). A 4-hour sliding window with a fixed 15-minute step is used. For each window, we compute several factors, including PSD_{WL} , f_{mid} , f_{peak} , and other parameters such as σ_c and $t_{adv} = (R - R_\odot)/V_r$. In total, 26,623 intervals were selected. As a first step, we cleaned the data, retaining only intervals where $0.005 < \delta t_{adv}/\langle t_{adv} \rangle < 0.2$, leaving us with 25,641 intervals (This criteria is chosen to avoid missing values and abrupt changes in solar wind speed. 982 intervals were filtered out). The values of $1/f_{mid}$ were then sorted by R , as shown in Figure 4(a).

The scatter plot in panel (a) appears highly chaotic. This is because, during solar maximum (starting from E10 in late 2021), the ecliptic solar wind consists of a complex mixture of slow and fast wind. The turbulence outer scale in the slow wind is typically observed at very low frequencies $\lesssim 10^{-4}$ Hz (Bruno et al. 2019), whereas in the fast wind, the low-frequency spectral breaks are often found around 10^{-2} Hz to 10^{-3} Hz (Bruno & Carbone 2013). As a result, even for the same R , the distribution of $1/f_{mid}$ remains highly dispersed. Nevertheless, the binned mean value of $1/f_{mid}$ decreases with decreasing R and drops to about 3 minutes.

A more suitable parameter for sorting $1/f_{mid}$ is the advection time, t_{adv} . This parameter can serve as a proxy for the ‘‘age’’ of the solar wind plasma, as fast wind naturally takes less time to reach a given R than slow wind. The scatter plot of $1/f_{mid}$ as a function of t_{adv} is shown in panel (c). When sorted by t_{adv} , the overall trend becomes much clearer: $1/f_{mid}$ steadily decreases from the saturation value (estimated from a Kolmogorov $f^{-5/3}$ spectrum, see Appendix A for details) to around 2 to 3 minutes.

What is more intriguing is the evolution of the Alfvén waves. In panels (b) and (d), we keep only the intervals where $|\sigma_c| > 0.75$, leaving 9125 intervals. Surprisingly, for both R and t_{adv} , the overall trends remain almost unchanged. To probe the evolution of $1/f_{mid}$ within a single stream, we highlight two long intervals from the two confirmed *in situ* coronal holes from the inbound of E10 (Badman et al. 2023) and E12 (Huang et al. 2024) (the dots are connected according to the value of R). Following a single stream originating from a coronal hole, $1/f_{mid}$ gradually drops toward 2 minutes as the ‘‘age’’ of the plasma decreases.

In summary, the trend of $1/f_{mid}$ as a function of t_{adv} is very clear. For the ‘‘youngest’’ solar wind, $1/f_{mid}$ drops to around 2 to 3 minutes. The trend remains largely unchanged when considering only the Alfvénic intervals, indicating that this is an intrinsic property of Alfvén waves originating from the base of the corona. In the next section, we will provide a detailed discussion on the nonlinear effects and the implications of our results.

5. DISCUSSION AND CONCLUSIONS

The trend in Figure 4(d) doesn’t seem to stabilize with t_{adv} . Indeed, both the E10 coronal hole in (d) and the cases in Figure 3 exhibit $1/f_{mid}$ values smaller than the smallest binned mean from the trend, closer to 2 minutes ($f_{mid} \approx 8.3$ mHz) rather than 3 minutes ($f_{mid} \approx 5.6$ mHz). We argue that the real saturation value of $1/f_{mid}$ is closer to 2 minutes from two perspectives: (1) the actual propagation time of the Alfvén

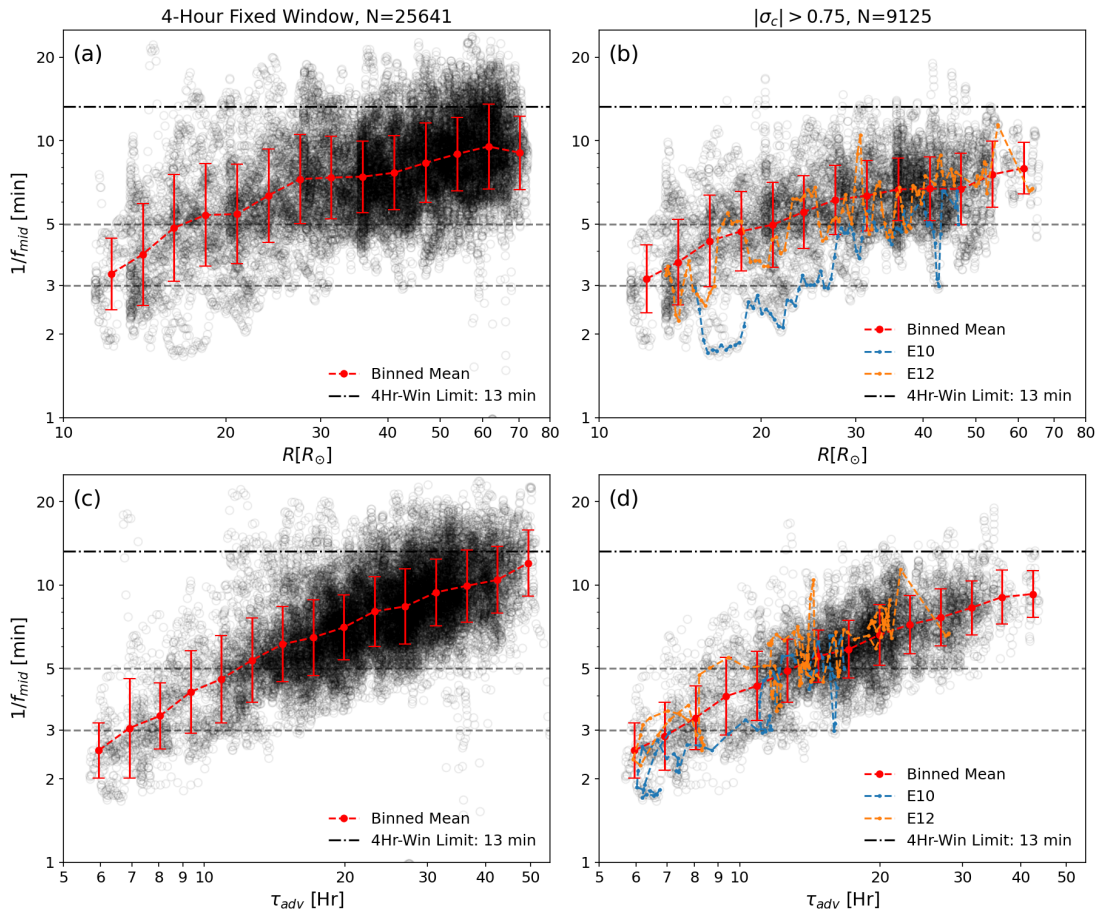


Figure 4. (a) Scatter plot of $1/f_{mid}$ as a function of heliocentric distance R . The window limit is the $1/f_{mid}$ value estimated from a Kolmogorov $f^{-5/3}$ spectrum. The errorbars indicate one standard deviation in logarithmic scale. (b) Intervals with $|\sigma_c| > 0.75$ are selected. The two known *in situ* coronal holes from E10 and E12 are highlighted. (c) $1/f_{mid}$ is plotted as a function of $t_{adv} = (R - R_\odot)/V_r$. (d) Intervals with $|\sigma_c| > 0.75$ are selected.

waves, and (2) the deformation and evolution of the turbulence spectrum.

The actual propagation time, t_{prop} , of the Alfvén waves from the base of the corona to the Alfvén surface is significantly shorter than t_{adv} :

$$t_{prop} = \int_{R_\odot}^{R_c} \frac{dR}{U + V_A} \quad (15)$$

where R_c is the heliocentric distance of the Alfvén surface. Using the profile in Figure 2, we estimate $t_{prop} \approx 1.84$ hr, which is much shorter than the smallest $t_{adv} \approx 5.7$ hr. This indicates that the “age” of the Alfvén waves in the intervals located at the lower left corner of panel (d) is much “younger” than it appears. In contrast, changes in t_{adv} more closely reflect variations in t_{prop} , particularly when t_{adv} is large. However, it is clear that a difference of 1.84 hours has little impact on the value of $1/f_{mid}$.

Furthermore, the shift of $1/f_{mid}$ to higher values with increasing t_{adv} likely results from two key effects in so-

lar wind turbulence: (1) the gradual deformation of the spectrum from “shallow-inertial” to “shallow- $1/f$ -inertial”, and eventually to “ $1/f$ -inertial” as the solar wind moves away from the Sun (Huang et al. 2023b; Davis et al. 2023). This transformation, proposed to be caused by the parametric decay-induced inverse cascade of Alfvén waves (Chandran 2018), typically generates a $1/f$ range starting from the “bend” that expands toward lower frequencies, gradually shifting $1/f_{mid}$ to the left; and (2) the cascade and dissipation of turbulent fluctuation energy, which consumes energy in the $1/f$ energy-containing range, pushing both the spectral break of the “ $1/f$ -inertial” spectrum and f_{mid} to lower frequencies (Tu & Marsch 1995; Bruno & Carbone 2013; Wu et al. 2020, 2021).

Both mechanisms drive $1/f_{mid}$ to larger values by “spreading out” the concentration of fluctuation energy toward lower frequencies. The “shallow-inertial” spectrum observed in the most pristine solar wind indicates a concentration of fluctuation energy. To shift $1/f_{mid}$ to

even smaller values, the spectrum as a whole would need to move toward higher frequencies, rather than simply deform. To our knowledge, no current turbulence transport theories or models predict such behavior. Therefore, we propose that the true saturation value of $1/f_{mid}$ is likely closer to 2 minutes.

We would also like to emphasize the importance of the rectification of the spectrum: $P(f) \cdot f$. For comparison, Kumar et al. (2023) analyzed proton velocity data from the coronal hole outflow in PSP E10 and discovered distinct period peaks around 3, 5, 10, and 20 minutes, consistent with the period peaks in the emission intensity of jetlets at the base of coronal hole plumes and plumelets (Uritsky et al. 2021; Kumar et al. 2022). However, in their wavelet analysis, the PSD was not rectified with the corresponding frequency, as suggested by Liu et al. (2007). Due to the high Alfvénicity of the coronal outflow, if rectified, the PSD from the proton velocity should resemble the trace magnetic PSD compiled in this study.

Our findings show a striking consistency with the remote sensing spectrum derived from the swaying motions of coronal structures observed by SDO/AIA within coronal holes. Specifically, in Figure 6(c) of Morton et al. (2015), the peak of the histogram for Alfvén(ic) wave periods falls between 100s and 200s. Furthermore, in Figure 1(d) of Morton et al. (2019), after rectifying the SDO/AIA coronal hole power spectral density (PSD) with f , the true peak of the spectrum emerges clearly at around 8 mHz (or approximately 2 minutes). However, this peak is absent in the PSD compiled from CoMP Doppler velocity time series. The authors noted that due to instrument uncertainties, they were unable to confirm the authenticity of this peak.

Finally, our results establish a strong connection between the Alfvén waves measured by PSP near the Alfvén surface and those launched from the base of the corona. The dominance of 2-minute Alfvén waves near the Alfvén surface suggests that the Alfvén waves in the solar wind could be the result of leakage from p-mode oscillations, as proposed by previous studies (Cally 2012; Hansteen & Velli 2012; Morton et al. 2013, 2015; Cally 2017; Morton et al. 2019). However, current evidence (Morton et al. 2019) is not yet robust enough to confirm this hypothesis. It is also possible that Alfvén waves at the corona’s base are generated by convective motions at the photosphere, which shake the footprints of open magnetic field lines (Cranmer & Ballegoijen 2005; Ballegoijen & Asgari-Targhi 2016). A detailed discussion to differentiate between these models is, unfortunately, beyond the scope of this study.

Future studies on this matter can focus on two avenues: First, PSP will reach its deepest perihelion in December 2024. The new data from deeper below the Alfvén surface will provide valuable insights into the evolution of the turbulence spectrum. Thus, a dedicated cross-validation study between *in situ* observations and remote sensing in the future is of great interest. Second, the origin of the energy-containing $1/f$ range has been debated for decades in the field (Keshner 1982; Montroull & Shlesinger 1982; Bak et al. 1987; Velli et al. 1989; Matthaeus & Goldstein 1986; Matthaeus et al. 2007; Bemporad et al. 2008; Dmitruk et al. 2011; Verdini et al. 2012; Matteini et al. 2018; Chandran 2018; Magyar & Doorsselaere 2022; Meyrand et al. 2023). A more detailed study on the evolution of the spectrum in the young solar wind will likely shed new light on this topic.

ACKNOWLEDGEMENTS

The authors acknowledge the following open-source packages: Lam et al. (2015); Harris et al. (2020); Hunter (2007); Angelopoulos et al. (2019); Virtanen et al. (2020). Z.H. thanks Pankaj Kumar for valuable discussions. This research was funded in part by the FIELDS experiment on the Parker Solar Probe spacecraft, designed and developed under NASA contract UCB #00010350/NASA NNN06AA01C, and the NASA Parker Solar Probe Observatory Scientist grant NASA NNX15AF34G, and NASA HTMS 80NSSC20K1275. M.V. acknowledges support from ISSI via the J. Geiss fellowship. B.C. acknowledges support from NASA grant 80NSSC24K0171. C.S. acknowledges supported from NSF SHINE #2229566 and NASA ECIP #80NSSC23K1064.

APPENDIX

A. POWER SPECTRUM DENSITY AND WINDOW LIMIT

Figure 5 is an illustration of the window limit of 13 minute for the 4-hour window (the dotted dashed line in Figure 4) and the definition of the lines are consistent with Figure 1(b). An artificial Kolmogorov spectrum $P(f) = f^{-5/3}$ is plotted with the orange line. The middle frequency f_{mid} is defined as the median value of the frequency range which contains the middle 50% of the total fluctuation energy.

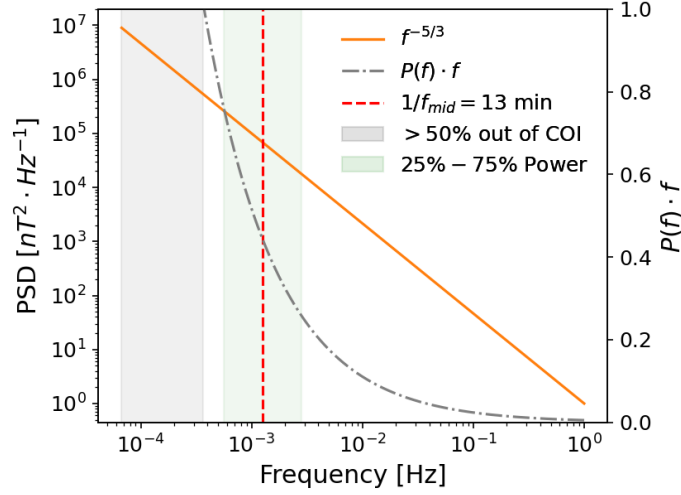


Figure 5. Illustration of the saturation $1/f_{mid}$ with a 4-hour window. Orange: Kolmogorov $P(f) = f^{-5/3}$ spectrum; Dotted dashed: Compensated spectrum $P(f) \cdot f$ in linear scale on twin axis; Gray area: Frequency range where $>50\%$ of points are out of the Cone of Influence; Green area: frequency range that contains 50% of fluctuation energy (from 25% to 75%).

REFERENCES

- Adhikari, L., Zank, G. P., Zhao, L.-L., et al. 2021, *Astronomy & Astrophysics*, 656, A6, doi: [10.1051/0004-6361/202140672](https://doi.org/10.1051/0004-6361/202140672)
- Alazraki, G., & Couturier, P. 1971, *Astronomy and Astrophysics*, Vol. 13, p. 380 (1971), 13, 380
- Andrés, N., Sahraoui, F., Huang, S., Hadid, L. Z., & Galtier, S. 2022, *Astronomy & Astrophysics*, 661, A116, doi: [10.1051/0004-6361/202142994](https://doi.org/10.1051/0004-6361/202142994)
- Angelopoulos, V., Cruce, P., Drozdov, A., et al. 2019, *Space Science Reviews*, 215, 9, doi: [10.1007/s11214-018-0576-4](https://doi.org/10.1007/s11214-018-0576-4)
- Badman, S. T., Riley, P., Jones, S. I., et al. 2023, *Journal of Geophysical Research: Space Physics*, 128, e2023JA031359, doi: [10.1029/2023JA031359](https://doi.org/10.1029/2023JA031359)
- Bak, P., Tang, C., & Wiesenfeld, K. 1987, *Physical Review Letters*, 59, 381, doi: [10.1103/PhysRevLett.59.381](https://doi.org/10.1103/PhysRevLett.59.381)
- Bale, S. D., Goetz, K., Harvey, P. R., et al. 2016, *fr*, 204, 49, doi: [10.1007/s11214-016-0244-5](https://doi.org/10.1007/s11214-016-0244-5)
- Bale, S. D., Badman, S. T., Bonnell, J. W., et al. 2019, *Nature*, 1, doi: [10.1038/s41586-019-1818-7](https://doi.org/10.1038/s41586-019-1818-7)
- Bale, S. D., Horbury, T. S., Velli, M., et al. 2021, *The Astrophysical Journal*, 923, 174, doi: [10.3847/1538-4357/ac2d8c](https://doi.org/10.3847/1538-4357/ac2d8c)
- Bale, S. D., Drake, J. F., McManus, M. D., et al. 2023, *Nature*, 618, 252, doi: [10.1038/s41586-023-05955-3](https://doi.org/10.1038/s41586-023-05955-3)
- Ballegooijen, A. A. v., & Asgari-Targhi, M. 2016, *The Astrophysical Journal*, 821, 106, doi: [10.3847/0004-637X/821/2/106](https://doi.org/10.3847/0004-637X/821/2/106)
- Bandyopadhyay, R., Matthaeus, W. H., McComas, D. J., et al. 2022, *The Astrophysical Journal Letters*, 926, L1, doi: [10.3847/2041-8213/ac4a5c](https://doi.org/10.3847/2041-8213/ac4a5c)
- Banerjee, D., Krishna Prasad, S., Pant, V., et al. 2021, *Space Science Reviews*, 217, 76, doi: [10.1007/s11214-021-00849-0](https://doi.org/10.1007/s11214-021-00849-0)
- Barnes, A., & Hollweg, J. V. 1974, *Journal of Geophysical Research*, 79, 2302, doi: [10.1029/JA079i016p02302](https://doi.org/10.1029/JA079i016p02302)
- Belcher, J. W. 1971, *Astrophysical Journal*, vol. 168, p.509, doi: [10.1086/151105](https://doi.org/10.1086/151105)
- Belcher, J. W., & Davis, L. 1971, *Journal of Geophysical Research*, 76, 3534, doi: [10.1029/JA076i016p03534](https://doi.org/10.1029/JA076i016p03534)
- Belcher, J. W., & Olbert, S. 1975, *The Astrophysical Journal*, 200, 369
- Bemporad, A., Matthaeus, W. H., & Poletto, G. 2008, *The Astrophysical Journal*, 677, L137, doi: [10.1086/588093](https://doi.org/10.1086/588093)
- Boldyrev, S. 2005, *The Astrophysical Journal*, 626, L37, doi: [10.1086/431649](https://doi.org/10.1086/431649)
- . 2006, *Physical Review Letters*, 96, 115002, doi: [10.1103/PhysRevLett.96.115002](https://doi.org/10.1103/PhysRevLett.96.115002)
- Bowen, T. A., Bale, S. D., Bonnell, J. W., et al. 2020, *Journal of Geophysical Research: Space Physics*, 125, e2020JA027813, doi: [10.1029/2020JA027813](https://doi.org/10.1029/2020JA027813)
- Bretherton, F. P. 1968, *Proceedings of the Royal Society of London. Series A. Mathematical and Physical Sciences*, 302, 529, doi: [10.1098/rspa.1968.0034](https://doi.org/10.1098/rspa.1968.0034)
- Bruno, R., & Carbone, V. 2013, *Living Reviews in Solar Physics*, 10, 2, doi: [10.12942/lrsp-2013-2](https://doi.org/10.12942/lrsp-2013-2)
- Bruno, R., Telloni, D., Sorriso-Valvo, L., et al. 2019, *Astronomy & Astrophysics*, 627, A96, doi: [10.1051/0004-6361/201935841](https://doi.org/10.1051/0004-6361/201935841)
- Cally, P. S. 2012, *Solar Physics*, 280, 33, doi: [10.1007/s11207-012-0052-3](https://doi.org/10.1007/s11207-012-0052-3)
- . 2017, *Monthly Notices of the Royal Astronomical Society*, 466, 413, doi: [10.1093/mnras/stw3215](https://doi.org/10.1093/mnras/stw3215)
- Chandran, B. D. G. 2018, *Journal of Plasma Physics*, 84, doi: [10.1017/S0022377818000016](https://doi.org/10.1017/S0022377818000016)
- Chandran, B. D. G., Schekochihin, A. A., & Mallet, A. 2015, *The Astrophysical Journal*, 807, 39, doi: [10.1088/0004-637X/807/1/39](https://doi.org/10.1088/0004-637X/807/1/39)
- Chen, C. H. K., Bale, S. D., Bonnell, J. W., et al. 2020, *The Astrophysical Journal Supplement Series*, 246, 53, doi: [10.3847/1538-4365/ab60a3](https://doi.org/10.3847/1538-4365/ab60a3)
- Chhiber, R., Pecora, F., Usmanov, A. V., et al. 2024, *Monthly Notices of the Royal Astronomical Society: Letters*, 533, L70, doi: [10.1093/mnrasl/slae051](https://doi.org/10.1093/mnrasl/slae051)
- Cranmer, S. R., & Ballegooijen, A. A. v. 2005, *The Astrophysical Journal Supplement Series*, 156, 265, doi: [10.1086/426507](https://doi.org/10.1086/426507)
- Davis, N., Chandran, B. D. G., Bowen, T. A., et al. 2023, *The Astrophysical Journal*, 950, 154, doi: [10.3847/1538-4357/acd177](https://doi.org/10.3847/1538-4357/acd177)
- De Pontieu, B., McIntosh, S. W., Carlsson, M., et al. 2007, *Science*, 318, 1574, doi: [10.1126/science.1151747](https://doi.org/10.1126/science.1151747)
- Dewar, R. L. 1970, *Physics of Fluids*, 13, 2710, doi: [10.1063/1.1692854](https://doi.org/10.1063/1.1692854)
- Dmitruk, P., Mininni, P. D., Pouquet, A., Servidio, S., & Matthaeus, W. H. 2011, *Physical Review E*, 83, 066318, doi: [10.1103/PhysRevE.83.066318](https://doi.org/10.1103/PhysRevE.83.066318)
- Drake, J. F., Agapitov, O., Swisdak, M., et al. 2021, *Astronomy & Astrophysics*, 650, A2
- Duan, D., He, J., Bowen, T. A., et al. 2021, *The Astrophysical Journal Letters*, 915, L8, doi: [10.3847/2041-8213/ac07ac](https://doi.org/10.3847/2041-8213/ac07ac)
- Dunn, C., Bowen, T., Mallet, A., Badman, S., & Bale, S. 2023, *Effect of Spherical Polarization on the Magnetic Spectrum of the Solar Wind*, arXiv, doi: [10.48550/arXiv.2305.09763](https://doi.org/10.48550/arXiv.2305.09763)

- Fox, N. J., Velli, M. C., Bale, S. D., et al. 2016, *Space Science Reviews*, 204, 7, doi: [10.1007/s11214-015-0211-6](https://doi.org/10.1007/s11214-015-0211-6)
- Goldreich, P., & Sridhar, S. 1995, *The Astrophysical Journal*, 438, 763, doi: [10.1086/175121](https://doi.org/10.1086/175121)
- . 1997, *\apj*, 485, 680, doi: [10.1086/304442](https://doi.org/10.1086/304442)
- Gringauz, K. I., Bezrukhikh, V. V., Ozerov, V. D., & Rybchinskii, R. E. 1962, *Planetary and Space Science*, 9, 103, doi: [10.1016/0032-0633\(62\)90180-0](https://doi.org/10.1016/0032-0633(62)90180-0)
- Hansen, S. C., & Cally, P. S. 2012, *The Astrophysical Journal*, 751, 31, doi: [10.1088/0004-637X/751/1/31](https://doi.org/10.1088/0004-637X/751/1/31)
- Hansteen, V. H., & Velli, M. 2012, *Space Science Reviews*, 172, 89, doi: [10.1007/s11214-012-9887-z](https://doi.org/10.1007/s11214-012-9887-z)
- Harris, C. R., Millman, K. J., van der Walt, S. J., et al. 2020, *Nature*, 585, 357, doi: [10.1038/s41586-020-2649-2](https://doi.org/10.1038/s41586-020-2649-2)
- Heinemann, M., & Olbert, S. 1980, *Journal of Geophysical Research: Space Physics*, 85, 1311, doi: [10.1029/JA085iA03p01311](https://doi.org/10.1029/JA085iA03p01311)
- Hollweg, J. V., Jackson, S., & Galloway, D. 1982, *Solar Physics*, 75, 35, doi: [10.1007/BF00153458](https://doi.org/10.1007/BF00153458)
- Horbury, T. S., Wicks, R. T., & Chen, C. H. K. 2012, *Space Science Reviews*, 172, 325, doi: [10.1007/s11214-011-9821-9](https://doi.org/10.1007/s11214-011-9821-9)
- Hou, C., He, J., Duan, D., et al. 2024, *Nature Astronomy*, 1, doi: [10.1038/s41550-024-02321-9](https://doi.org/10.1038/s41550-024-02321-9)
- Huang, J., Kasper, J. C., Fisk, L. A., et al. 2023a, *The Astrophysical Journal*, 952, 33, doi: [10.3847/1538-4357/acd17e](https://doi.org/10.3847/1538-4357/acd17e)
- Huang, Z., Sioulas, N., Shi, C., et al. 2023b, *The Astrophysical Journal Letters*, 950, L8, doi: [10.3847/2041-8213/acd7f2](https://doi.org/10.3847/2041-8213/acd7f2)
- Huang, Z., Shi, C., Velli, M., et al. 2024, *The Astrophysical Journal Letters*, 973, L26, doi: [10.3847/2041-8213/ad72f1](https://doi.org/10.3847/2041-8213/ad72f1)
- Hunter, J. D. 2007, *Computing in Science & Engineering*, 9, 90, doi: [10.1109/MCSE.2007.55](https://doi.org/10.1109/MCSE.2007.55)
- Iroshnikov, P. S. 1964, *\sovast*, 7, 566
- Jagarlamudi, V. K., Raouafi, N. E., Bourouaine, S., et al. 2023, *The Astrophysical Journal Letters*, 950, L7, doi: [10.3847/2041-8213/acd778](https://doi.org/10.3847/2041-8213/acd778)
- Jess, D. B., Mathioudakis, M., Erdélyi, R., et al. 2009, *Science*, 323, 1582, doi: [10.1126/science.1168680](https://doi.org/10.1126/science.1168680)
- Jess, D. B., Morton, R. J., Verth, G., et al. 2015, *Space Science Reviews*, 190, 103, doi: [10.1007/s11214-015-0141-3](https://doi.org/10.1007/s11214-015-0141-3)
- Kasper, J. C., Abiad, R., Austin, G., et al. 2016, *\fr*, 204, 131, doi: [10.1007/s11214-015-0206-3](https://doi.org/10.1007/s11214-015-0206-3)
- Kasper, J. C., Bale, S. D., Belcher, J. W., et al. 2019, *Nature*, 576, 228
- Kasper, J. C., Klein, K. G., Lichko, E., et al. 2021, *Physical Review Letters*, 127, 255101, doi: [10.1103/PhysRevLett.127.255101](https://doi.org/10.1103/PhysRevLett.127.255101)
- Keshner, M. 1982, *Proceedings of the IEEE*, 70, 212, doi: [10.1109/PROC.1982.12282](https://doi.org/10.1109/PROC.1982.12282)
- Kraichnan, R. 1965, doi: [10.1063/1.1761412](https://doi.org/10.1063/1.1761412)
- Kruparova, O., Krupar, V., Szabo, A., Pulupa, M., & Bale, S. D. 2023, *The Astrophysical Journal*, 957, 13, doi: [10.3847/1538-4357/acf572](https://doi.org/10.3847/1538-4357/acf572)
- Kumar, P., Karpen, J. T., Uritsky, V. M., et al. 2022, *The Astrophysical Journal*, 933, 21, doi: [10.3847/1538-4357/ac6c24](https://doi.org/10.3847/1538-4357/ac6c24)
- . 2023, *The Astrophysical Journal Letters*, 951, L15, doi: [10.3847/2041-8213/acd54e](https://doi.org/10.3847/2041-8213/acd54e)
- Kuniyoshi, H., Shoda, M., Morton, R. J., & Yokoyama, T. 2023, doi: [10.48550/ARXIV.2311.16461](https://doi.org/10.48550/ARXIV.2311.16461)
- Kuridze, D., & Zaqarashvili, T. 2008, *Journal of Atmospheric and Solar-Terrestrial Physics*, 70, 351, doi: [10.1016/j.jastp.2007.08.059](https://doi.org/10.1016/j.jastp.2007.08.059)
- Lam, S. K., Pitrou, A., & Seibert, S. 2015, in *Proceedings of the Second Workshop on the LLVM Compiler Infrastructure in HPC (Austin Texas: ACM)*, 1–6, doi: [10.1145/2833157.2833162](https://doi.org/10.1145/2833157.2833162)
- Larosa, A., Chen, C. H. K., McIntyre, J. R., & Jagarlamudi, V. K. 2023, *The relation between magnetic switchbacks and turbulence in the inner heliosphere*, *arXiv*, doi: [10.48550/arXiv.2312.16521](https://doi.org/10.48550/arXiv.2312.16521)
- Larosa, A., Krasnoselskikh, V., Wit, T. D. d., et al. 2021, *Astronomy & Astrophysics*, 650, A3, doi: [10.1051/0004-6361/202039442](https://doi.org/10.1051/0004-6361/202039442)
- Leer, E., & Holzer, T. E. 1980, *Journal of Geophysical Research: Space Physics*, 85, 4681, doi: [10.1029/JA085iA09p04681](https://doi.org/10.1029/JA085iA09p04681)
- Liu, M., Issautier, K., Meyer-Vernet, N., et al. 2021a, *Astronomy & Astrophysics*, 650, A14, doi: [10.1051/0004-6361/202039615](https://doi.org/10.1051/0004-6361/202039615)
- Liu, M., Issautier, K., Moncuquet, M., et al. 2023, *Astronomy & Astrophysics*, 674, A49, doi: [10.1051/0004-6361/202245450](https://doi.org/10.1051/0004-6361/202245450)
- Liu, Y., Liang, X. S., & Weisberg, R. H. 2007, *Journal of Atmospheric and Oceanic Technology*, 24, 2093, doi: [10.1175/2007JTECHO511.1](https://doi.org/10.1175/2007JTECHO511.1)
- Liu, Y. D., Chen, C., Stevens, M. L., & Liu, M. 2021b, *The Astrophysical Journal Letters*, 908, L41, doi: [10.3847/2041-8213/abe38e](https://doi.org/10.3847/2041-8213/abe38e)
- Magyar, N., & Doorsselaere, T. V. 2022, *The Astrophysical Journal*, 938, 98, doi: [10.3847/1538-4357/ac8b81](https://doi.org/10.3847/1538-4357/ac8b81)
- Matteini, L., Horbury, T. S., Neugebauer, M., & Goldstein, B. E. 2014, *Geophysical Research Letters*, 41, 259, doi: [10.1002/2013GL058482](https://doi.org/10.1002/2013GL058482)
- Matteini, L., Stansby, D., Horbury, T. S., & Chen, C. H. K. 2018, *The Astrophysical Journal*, 869, L32, doi: [10.3847/2041-8213/aaf573](https://doi.org/10.3847/2041-8213/aaf573)

- Matteini, L., Tenerani, A., Landi, S., et al. 2024, *Physics of Plasmas*, 31, 032901, doi: [10.1063/5.0177754](https://doi.org/10.1063/5.0177754)
- Matthaeus, W. H. 2021, *Physics of Plasmas*, 28, 032306, doi: [10.1063/5.0041540](https://doi.org/10.1063/5.0041540)
- Matthaeus, W. H., Breech, B., Dmitruk, P., et al. 2007, *The Astrophysical Journal*, 657, L121, doi: [10.1086/513075](https://doi.org/10.1086/513075)
- Matthaeus, W. H., & Goldstein, M. L. 1986, *Physical Review Letters*, 57, 495, doi: [10.1103/PhysRevLett.57.495](https://doi.org/10.1103/PhysRevLett.57.495)
- McIntyre, J. R., Chen, C. H., & Larosa, A. 2023, *The Astrophysical Journal*, 957, 111. <https://iopscience.iop.org/article/10.3847/1538-4357/acf3dd/meta>
- Meyrand, R., Squire, J., Mallet, A., & Chandran, B. D. G. 2023, Reflection-driven turbulence in the super-Alfvénic solar wind, arXiv, doi: [10.48550/arXiv.2308.10389](https://arxiv.org/abs/10.48550/arXiv.2308.10389)
- Moncuquet, M., Meyer-Vernet, N., Issautier, K., et al. 2020, *The Astrophysical Journal Supplement Series*, 246, 44, doi: [10.3847/1538-4365/ab5a84](https://doi.org/10.3847/1538-4365/ab5a84)
- Montroll, E. W., & Shlesinger, M. F. 1982, *Proceedings of the National Academy of Sciences of the United States of America*, 79, 3380, doi: [10.1073/pnas.79.10.3380](https://doi.org/10.1073/pnas.79.10.3380)
- Morton, R. J., Sharma, R., Tajfirouze, E., & Miriyala, H. 2023, *Reviews of Modern Plasma Physics*, 7, 17, doi: [10.1007/s41614-023-00118-3](https://doi.org/10.1007/s41614-023-00118-3)
- Morton, R. J., Tomczyk, S., & Pinto, R. 2015, *Nature Communications*, 6, 7813, doi: [10.1038/ncomms8813](https://doi.org/10.1038/ncomms8813)
- Morton, R. J., Verth, G., Fedun, V., Shelyag, S., & Erdélyi, R. 2013, *The Astrophysical Journal*, 768, 17, doi: [10.1088/0004-637X/768/1/17](https://doi.org/10.1088/0004-637X/768/1/17)
- Morton, R. J., Weberg, M. J., & McLaughlin, J. A. 2019, *Nature Astronomy*, 3, 223, doi: [10.1038/s41550-018-0668-9](https://doi.org/10.1038/s41550-018-0668-9)
- Mostafavi, P., Allen, R. C., McManus, M. D., et al. 2022, *The Astrophysical Journal Letters*, 926, L38, doi: [10.3847/2041-8213/ac51e1](https://doi.org/10.3847/2041-8213/ac51e1)
- Neugebauer, M., & Snyder, C. W. 1966, *Journal of Geophysical Research (1896-1977)*, 71, 4469, doi: [10.1029/JZ071i019p04469](https://doi.org/10.1029/JZ071i019p04469)
- Oughton, S., Matthaeus, W. H., Wan, M., & Osman, K. T. 2015, *Philosophical Transactions of the Royal Society A: Mathematical, Physical and Engineering Sciences*, doi: [10.1098/rsta.2014.0152](https://doi.org/10.1098/rsta.2014.0152)
- Parker, E. N. 1958, *The Astrophysical Journal*, 128, 664, doi: [10.1086/146579](https://doi.org/10.1086/146579)
- . 1965, *Space Science Reviews*, 4, 666, doi: [10.1007/BF00216273](https://doi.org/10.1007/BF00216273)
- Perez, J. C., Bourouaine, S., Chen, C. H. K., & Raouafi, N. E. 2021, *Astronomy & Astrophysics*, 650, A22, doi: [10.1051/0004-6361/202039879](https://doi.org/10.1051/0004-6361/202039879)
- Raouafi, N. E., Matteini, L., Squire, J., et al. 2023, *Space Science Reviews*, 219, 8, doi: [10.1007/s11214-023-00952-4](https://doi.org/10.1007/s11214-023-00952-4)
- Rieutord, M., Roudier, T., Rincon, F., et al. 2010, *Astronomy & Astrophysics*, 512, A4, doi: [10.1051/0004-6361/200913303](https://doi.org/10.1051/0004-6361/200913303)
- Rivera, Y. J., Badman, S. T., Stevens, M. L., et al. 2024, *Science*, 385, 962, doi: [10.1126/science.adk6953](https://doi.org/10.1126/science.adk6953)
- Shi, C., Velli, M., Bale, S. D., et al. 2022a, *Physics of Plasmas*, 29, 122901, doi: [10.1063/5.0124703](https://doi.org/10.1063/5.0124703)
- Shi, C., Velli, M., Panasenco, O., et al. 2021, *Astronomy & Astrophysics*, 650, A21, doi: [10.1051/0004-6361/202039818](https://doi.org/10.1051/0004-6361/202039818)
- Shi, C., Panasenco, O., Velli, M., et al. 2022b, *The Astrophysical Journal*, 934, 152, doi: [10.3847/1538-4357/ac7c11](https://doi.org/10.3847/1538-4357/ac7c11)
- Sioulas, N., Huang, Z., Velli, M., et al. 2022, *The Astrophysical Journal*, 934, 143, doi: [10.3847/1538-4357/ac7aa2](https://doi.org/10.3847/1538-4357/ac7aa2)
- Sioulas, N., Velli, M., Huang, Z., et al. 2023a, *The Astrophysical Journal*, 951, 141. <https://iopscience.iop.org/article/10.3847/1538-4357/acc658/meta>
- Sioulas, N., Huang, Z., Shi, C., et al. 2023b, *The Astrophysical Journal Letters*, 943, L8, doi: [10.3847/2041-8213/acaef7](https://doi.org/10.3847/2041-8213/acaef7)
- Taylor, G. I. 1938, *Proceedings of the Royal Society of London Series A*, 164, 476, doi: [10.1098/rspa.1938.0032](https://doi.org/10.1098/rspa.1938.0032)
- Telloni, D., Zank, G. P., Stangalini, M., et al. 2022, *The Astrophysical Journal Letters*, 936, L25, doi: [10.3847/2041-8213/ac8104](https://doi.org/10.3847/2041-8213/ac8104)
- Tian, H., DeLuca, E. E., Cranmer, S. R., et al. 2014, *Science*, 346, 1255711, doi: [10.1126/science.1255711](https://doi.org/10.1126/science.1255711)
- Tsurutani, B. T., Ho, C. M., Arballo, J. K., et al. 1997, *Plasma Physics and Controlled Fusion*, 39, A237, doi: [10.1088/0741-3335/39/5A/022](https://doi.org/10.1088/0741-3335/39/5A/022)
- Tu, C. Y., & Marsch, E. 1995, *Space Science Reviews*, 73, 1, doi: [10.1007/BF00748891](https://doi.org/10.1007/BF00748891)
- Ulrich, R. K. 1970, *The Astrophysical Journal*, 162, 993, doi: [10.1086/150731](https://doi.org/10.1086/150731)
- Unti, T. W. J., & Neugebauer, M. 1968, *The Physics of Fluids*, 11, 563, doi: [10.1063/1.1691953](https://doi.org/10.1063/1.1691953)
- Uritsky, V. M., DeForest, C. E., Karpen, J. T., et al. 2021, *The Astrophysical Journal*, 907, 1, doi: [10.3847/1538-4357/abd186](https://doi.org/10.3847/1538-4357/abd186)
- Velli, M. 1993, *Astronomy and Astrophysics*, 270, 304. <https://ui.adsabs.harvard.edu/abs/1993A&A...270..304V>
- Velli, M., Grappin, R., & Mangeney, A. 1989, *Physical Review Letters*, 63, 1807, doi: [chan](https://doi.org/10.1103/PhysRevLett.63.1807)
- . 1991, *Geophysical & Astrophysical Fluid Dynamics*, 62, 101, doi: [10.1080/03091929108229128](https://doi.org/10.1080/03091929108229128)
- Verdini, A., Grappin, R., Pinto, R., & Velli, M. 2012, *The Astrophysical Journal*, 750, L33, doi: [10.1088/2041-8205/750/2/L33](https://doi.org/10.1088/2041-8205/750/2/L33)

- Virtanen, P., Gommers, R., Oliphant, T. E., et al. 2020, Nature Methods, 17, 261, doi: [10.1038/s41592-019-0686-2](https://doi.org/10.1038/s41592-019-0686-2)
- Wu, H., Tu, C., Wang, X., He, J., & Yang, L. 2020, The Astrophysical Journal Letters, 904, L8, doi: [10.3847/2041-8213/abc5b6](https://doi.org/10.3847/2041-8213/abc5b6)
- Wu, H., Tu, C., Wang, X., et al. 2021, The Astrophysical Journal, 912, 84, doi: [10.3847/1538-4357/abf099](https://doi.org/10.3847/1538-4357/abf099)
- Zank, G. P., Zhao, L.-L., Adhikari, L., et al. 2022, The Astrophysical Journal Letters, 926, L16, doi: [10.3847/2041-8213/ac51da](https://doi.org/10.3847/2041-8213/ac51da)
- Zhang, J., Huang, S. Y., Yuan, Z. G., et al. 2022a, The Astrophysical Journal, 937, 70, doi: [10.3847/1538-4357/ac8c34](https://doi.org/10.3847/1538-4357/ac8c34)
- Zhang, J., Huang, S. Y., He, J. S., et al. 2022b, The Astrophysical Journal Letters, 924, L21, doi: [10.3847/2041-8213/ac4027](https://doi.org/10.3847/2041-8213/ac4027)
- Zhao, S. Q., Yan, H., Liu, T. Z., Liu, M., & Shi, M. 2021, The Astrophysical Journal, 923, 253. <https://iopscience.iop.org/article/10.3847/1538-4357/ac2ffe/meta>
- Zheng, X., Liu, K., Martinović, M. M., et al. 2024, The Astrophysical Journal, 963, 154, doi: [10.3847/1538-4357/ad236d](https://doi.org/10.3847/1538-4357/ad236d)